Energy Reports 11 (2024) 4523–4536

Contents lists available at ScienceDirect

Energy Reports

journal homepage: www.elsevier.com/locate/egyr

Research paper

Feasibility of high temperature superconducting cables for energy harvesting in large space-based solar power satellite applications: Electromagnetic, thermal and cost considerations

Alireza Sadeghi [a], Antonio Morandi [b], Mohammad Yazdani-Asrami [a,*]

[a] Propulsion, Electrification & Superconductivity Group, James Watt School of Engineering, University of Glasgow, Glasgow G12 8QQ, United Kingdom
[b] Department of Electrical, Electronic, and Information Engineering, University of Bologna, Viale del Risorgimento 2, Bologna 40136, Italy

ARTICLE INFO

Keywords:
Clean energy
Cost of energy
Power cable
Power loss
Space
Solar energy
Solar satellite
Weight

ABSTRACT

The aim of this paper is to present feasibility of application of High Temperature Superconducting (HTS) cables for Space-Based Solar Power (SBSP) application. SBSP is a promising technology that can deliver an infinite amount of clean and eco-friendly energy to the Earth. To deliver the harvested solar energy to the power systems on Earth, efficient energy transmission is critically important. To address the challenges of conventional transmission means, an ideal solution would be using HTS cables. In this research, the design procedure of a Direct Current (DC) HTS cable considering electromagnetic, thermal, and cost constraints is presented. The study considered a 2 MW bipolar DC HTS cable in five operational temperatures: 20 K, 30 K, 50 K, 65 K, and 77 K. The results were showed that the cost and weight of the designed HTS cables were increased by operational temperature increase. However, the cooling cost of HTS cable in higher temperatures, was less than lower temperatures. Also, the total efficiency of the HTS cable and cooling system were increased, when operational temperatures were changed from 20 K to 77 K, from 99.70% to 99.97%, respectively.

1. Introduction

High Temperature Superconducting (HTS) cables offer a wide range of advantages over their conventional copper-based counterparts, such as high current carrying capability in compacter and lighter structure (Yazdani-Asrami et al., 2022a). Direct Current (DC) HTS cables could transmit electrical energy with negligible loss, making them excellent choices for high current and low voltage purposes (Morandi, 2015a). Thus, DC HTS cables have been considered a promising futuristic option in some industries as reliable transmission/distribution lines, such as in conventional power grids (Sytnikov et al., 2016; Sadeghi et al., 2021), novel power grids with renewable energy resources (Klöppel et al., 2021; Sadeghi et al., 2022), cryo-electric aircraft (Sadeghi and Yazdani-Asrami, 2022; Yazdani-Asrami et al., 2023; Marchionini et al., 2017), electric ships (Cheetham et al., 2019), etc. In electric spacecraft and satellites, cryogenic cooling systems have been already implemented in the last few decades (Vorreiter, 1980). As a result of this, recently the possibility of implementing superconducting devices in space applications have been investigated. In this regard, superconducting coils and magnets have been used for galactic cosmic ray shielding (Kervendal et al., 2009; Bergen et al., 2016; Chesny et al., 2020; Calvelli et al., 2020), also for different types of electromagnetic thrusters (Ma et al., 2022; Yang et al., 2020; Cassady et al., 2009), and for magnetic bearing (Matsumura et al., 2016; Jiqiang et al., 2012). Thus, the advantages of HTS cables in terms of mass and loss (including the required cryogenic cooling system), make electric spacecraft a potential application for DC HTS cables to distribute the required electrical power for the thrust/propulsion of spacecraft and satellites.

It is estimated that by the end of 2050, the global demand for electrical energy will increase above 300%, reaching to more than 50 billion MWh (Groll, 2023; Kamani and Ardehali, 2023; Hasanuzzaman et al., 2017). To meet such a large demand, 2000–7000% more mining and construction works are required to build renewable power plants such as solar farms and windfarms and develop other clean energy resources. As a result of this, it raises concerns about available resources and the

Abbreviations: HTS, High Temperature Superconducting; SBSP, Space-Based Solar Power; DC, Direct Current; MWh, Mega Watt Hours; CO2, Carbon Dioxide; RF, Radio Frequency; KV, Kilo Volt; ReBCO, Rare Earth Barium Copper Oxide; EUR, Euro; LH_2, Liquid Hydrogen, GHe, Gaseous Helium; LN_2, Liquid Nitrogen; XLPE, Cross-linked polyethylene.

* Corresponding author.
E-mail address: mohammad.yazdani-asrami@glasgow.ac.uk (M. Yazdani-Asrami).

https://doi.org/10.1016/j.egyr.2024.04.023
Received 31 January 2024; Received in revised form 17 March 2024; Accepted 14 April 2024
Available online 24 April 2024

Nomenclatures

Symbols

K	Kelvin
δ_f	Former Thickness (m)
r_f	Radius of the Former (m)
ω_{sc}	width of superconducting tape (m)
α	winding angle (radian)
g	gap between HTS tapes (m)
R_f	Resistance of the former (Ω)
ρ_f	Resistivity of the former (Ω.m)
T_{op}	Operational Temperature (K)
L_C	cable length (m)
N_e	electrical number of HTS tapes
I_{op}	Operational current (A)
I_c	Critical Current (A)
$N_{g,i}$	Geometrical Number of HTS tapes in ith layer
P_f	perimeter previous layer (m)
m	Marginal Factor<1
δ_{ins}	Insulation thickness (m)
δ_{sc_i}	HTS tape thickness (m)
η	safety factor
E_b	breakdown voltage of insulation (V/m)
r_{ins_i}	Insulation outer radius (m)
V_{dc}	Operational DC voltage (V)
Q_t	Total Loss (W)
$Q_{NL_{SC}}$	loss originated in the superconductor (W/m)
Q_{vR}	pseudo insulation loss (W/m)
Q_{C_R}	pseudo-AC loss (W/m)
Q_{Cry}	Cryostat loss (W/m)
Q_{CL}	Current Lead Loss (W)
Q_{fo}	Former Loss (W)
n	Index Value
E_c	Critical Electric Field (V/m)
f_R	ripple frequency (Hz)
$\tan\delta$	Insulation loss factor
Cap_{ins}	Capacitance of insulation (F)
ΔU	half of full amplitude of voltage ripples at a given frequency (V)
ρ_{cu}	resistivity of copper current leads (Ω.m)
$P_{cooling}$	cooling power (W)
D_{YBCO}	Density of ReBCO Tape (kg/m^3)
k_{ReBCO}	Thermal conductivity of ReBCO Tape (W/m.K)
W_{fo}	Former Weight (kg)
W_{ins}	Insulation Weight (kg)
W_{CF}	Coolant Fluid Weight (kg)
C_{fo}	Cost of former (EUR)
L_{HTS_i}	Length of HTS tape (m)
cb_{HTS}	Base cost of HTS tapes $\left(\frac{EUR}{m}\right)$
cb_{ins}	Base cost of insulation $\left(\frac{EUR}{m}\right)$
cb_{sh}	Base cost of shield $\left(\frac{EUR}{m}\right)$
C_{vac}	Vacuum cost (EUR)
C_{term}	Termination cost (EUR)
C_{man}	maintenance cost (EUR)
C_{dis}	Discount cost (EUR)
Φ	Discount Rate
K_{core}	conductivity of cable aluminum/copper cable core
I_{RA}	ripple current amplitude
T_{amb}	ambient temperature (K)
$M_{cooling}$	mass of cooling system
$C_{P_{YBCO}}$	Heat Capacity of ReBCO Tape (J/kg.K)
D_{fo}	Former Density (kg/m^3)
W_{HTS_i}	HTS layers weight (kg)
W_{shield}	Shield Weight (kg)
W_{tot}	Total Weight of HTS cable (kg)
$C_{HTS_{i,j}}$	Cost of HTS tape (EUR)
cb_{fo}	base cost of copper former (cb_{fo}) $\left(\frac{EUR}{kg}\right)$
C_{ins}	Cost of insulation (EUR)
C_{shield}	Shield Layer Cost (EUR)
C_{other}	Other costs (EUR)
C_{cab}	Cabling cost (EUR)
C_{lay}	Laydown cost (EUR)
sy	Service year
C_{cryo}	Cryostat cost (EUR)
D_{CF}	Density pf coolant fluid (kg/m^3)
ΔU_c	maximum allowable voltage drops

environmental impacts of such exponential growth in mining and construction activities. On the other hand, the utilization of renewable energy resources on Earth is hindered by multiple factors. Firstly, energy storage technologies must be improved to increase the reliability and stability of power supplied to end users. Additionally, the initial costs of setting up renewable power infrastructure are considerably high. Moreover, some renewable-related technologies still have low Technology Readiness Level (TRL), and this brings further challenges for the energy sector (Anon Space Energy Initiative). One of the promising solutions is Space-Based Solar Power (SBSP). As shown in Fig. 1, this method considers harvesting the infinite solar energy existed in space and transmitting it wirelessly to the (Anon Space Energy Initiative) Earth. As shown in this figure, the SBSP consist of multiple solar panels that harvest the energy of the sun and use RF generators to transmit them to the Earth.

The implementation of SBSP, as an alternative to the conventional terrestrial renewable electrical energy production, could potentially reduce the burden of the increasing need for fossil fuels, water sources, metals, minerals, and more importantly CO_2 emissions and other pollutions for generating electric power in existing powerplants on the Earth (Ren et al., 2023). The SBSP technology has the advantage of continuous energy generation independent of the daylight hours or the weather conditions, that could enhance the safety and reliability of the power grid by removing the power generation uncertainties (Bidkar, 2012). Also, the consistency and intensity of the solar power in space is much higher than terrestrial solar farms that results in enhancing the energy generation per unit area of SBSP, compared to ground-based solar farms (Li et al., 2017a). It should be mentioned that terrestrial solar farms require a specific area for their implementation and installation that is limited by other land uses such as agriculture or urban developments. On the other hand, the SBSP technology does not have such limitation since it uses space in orbit, leaving land free for other purposes. Also, SBSP technology is less susceptible to natural disasters such as earthquakes, hurricanes, and floods. Finally, solar panels of SBSP, unlike those in ground applications, are not affected by extreme temperatures, or degradation from dust/pollution that results in longer lifetime of solar panels in SBSP technology (Verduci et al., 2022; Gosavi et al., 2021; Wood and Gilbert, 2022; Jenkins, 2011).

Regarding the challenges of SBSP technology, it is necessary to mention that the required technology for harvesting solar energy in space, transmitting it to Earth, and efficiently distributing it, is complex and costly. Enormous infrastructures and a robust transmission system are needed to make SBSP operational for green energy purposes in future. Although it offers a wide range of opportunities to address the

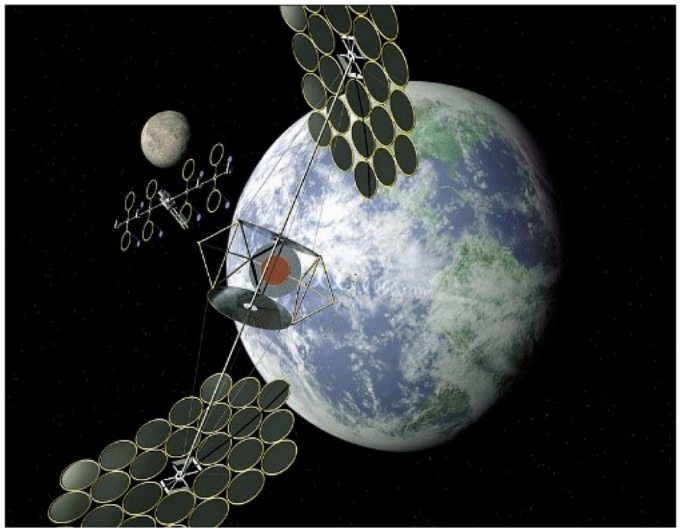

Fig. 1. A figurative picture of Space-Based Solar Power (SBSP) (Anon Space Energy Initiative) system.

challenges of conventional renewable energy systems, the economic, technical, and environmental considerations of such energy sources are critically important (Anon Space Energy Initiative). Indeed, SBSP is one of the satellite systems designed to harvest the energy of the sun in the form of electrical energy, by using solar panels. The collected electrical energy is then transmitted to Radio Frequency (RF) generators, where it undergoes conversion into high frequency waves. To ensure the energy reaches our planet, beams are employed to transmit these waves back to Earth (Li et al., 2017b). Once the waves reach Earth, they are converted back into electrical energy before being integrated into the power network for widespread use. This innovative concept proposes several significant advantages, making it a compelling prospect for future energy solutions. In this regard, High Temperature Superconducting (HTS) cable technology could be used as an efficient and cost-effective solution in SBSP. Energy from the sun is generated with low voltage and extremely high current (Jaffe and McSpadden, 2013). If one tends to use conventional copper-based transmission lines, as a connection between solar panels and RF generators, the final cost, size, and weight of such lines as well as their feasibility would be impractical for SBSP. HTS cables can drastically reduce the size, loss, weight, and cost of distribution lines in SBSP (Powell et al., 2002). Although HTS cables seem to be an excellent choice, there is a lack of investigation into the design and modelling of such cables for SBSP application. On the other hand, currently, researchers are well focused on developing solar cells with high efficiency by using the technologies like multi-junction solar cells to increase the power density of the energy harvesting part of the SBSPs. To further increase of the power density, investigations are carrying out to reduce the weight and size of the solar cells (Chiu, 2023; De Oliveira Lorenzi and Neves Micha, 2023; Liu et al., 2024). Regarding solar cells, flexible solar cells is also getting investigated since they are more convenient for packaging during launch and can be deployed easily in space (Liu et al., 2023; Cai et al., 2023; Qian et al., 2023). However, the implementation of superconducting devices for SBSP application has remained in very initial conceptual stages. Among the superconducting devices, HTS cables are critically important to deliver the high current/low voltage characteristic of the harvested energy to RF generators. The design of HTS cables have been discussed for power system applications and for aircraft applications, however; there is a gap in providing a design procedure for HTS cables considering the SBSP limitations and requirements.

In this paper, the design procedure of DC HTS cables for SBSP applications is presented by considering five different operational temperatures of 20 K, 30 K, 50 K, 65 K, and 77 K. In this study, the cost of HTS cable and cooling system, its weight, and temperature/AC loss characteristic are analysed to assess the feasibility of using HTS cables in SBSP applications. The findings indicate that the cost and weight of the designed HTS cables increase with higher operational temperatures. However, the cooling expenses for these cables at higher temperatures were lower compared to lower temperatures. Additionally, the overall efficiency of both the HTS cable and cooling system improved as operational temperatures rose from 20 K to 77 K, increasing from 99.70% to 99.97% respectively.

In this regard, Section 2 of the paper is dedicated to presenting the design routine of the HTS cable concerning the different layers in the HTS cable. Section three summarizes the analytical modelling approaches to characterize the electromagnetic and thermal behaviour of the cable. Finally, Section 4 of the paper is dedicated to the results of the design and modelling of the HTS cable. In this section firstly, the HTS cable is characterized and then, based on different temperatures, the final design of the cable is presented. At last, the design and efficiency of the HTS cable are comprised of copper and aluminium cables to show their inability to be implemented in the SBSP power system. Generally, after the design and magnetic, electric, and thermal characteristics of each HTS cable design, the cost and weight of these designs would be calculated and compared.

2. Design procedure of HTS cable

In this section, the design procedure of a DC HTS cable is presented based on the design requirements of the SBSP application. A schematic of a DC HTS cable is shown in Fig. 2, an DC HTS power cable consists of one or more layers of HTS tapes helically wound on a cylindrical stranded copper former surrounded by electrical insulation. As for conventional cables, a further copper layer, referred to the shield layer, is applied after the insulation to equalize the electric field. To reach the cryogenic operating temperature of the superconductor the whole HTS cable's core (former, HTS layers, insulation, and shield) is immersed in a double-wall cryostat allowing the flow of cryogenic coolant. After considering the power, voltage, and the current of DC HTS cable, the first step for the design of the cable is to calculate the thickness and radius of the former which is also used as the coolant return path. Then, there is one of the two poles of the bipolar HTS layers and then insulation. After that, the other pole is located on the insulation, then, there is a copper shield and cryostat.

In this regard, the thickness δ_f of former layers is 1 mm (about 0.04 in) which provides an acceptable fault limitation capability and minimizes the total weight of formers, based on the results shown in (Sadeghi and Yazdani-Asrami, 2022; Sato et al., 1997). Then, based on the width of the selected HTS tape, the radius of the former layer is selected based on Eq. (1) (Morandi, 2015b):

$$r_f \geq \frac{\omega_{sc} + g}{\sin\alpha \times \pi} \tag{1}$$

where, r_f is the radius of the former, ω_{sc} is the width of superconducting tape, α is the winding angle, and g is is the gap between HTS tapes.

The next step is to calculate the DC resistance of the former, based on its structural properties and according to Eq. (2) (Sumption et al., 2020):

$$R_f(T_{op}) = \frac{\rho_f(T_{op}) \quad L_C}{\pi\left(2\delta_f r_f - \delta_f^2\right)} \tag{2}$$

where, $R_f(T_{op})$ and $\rho_f(T_{op})$ are the resistance and resistivity of the former in operating temperature of T_{op}, L_C is cable length, δ_f is the thickness of the former layer, and r_f is the radius of the former layer.

Eq. (3) shows the number of HTS tapes N_e in the cable that is electrically required to carry the operating current of I_{op} in DC HTS cable, in each pole, while Eq. (4) shows the number of HTS tapes on each former that is geometrically possible (Kottonau et al., 2019).

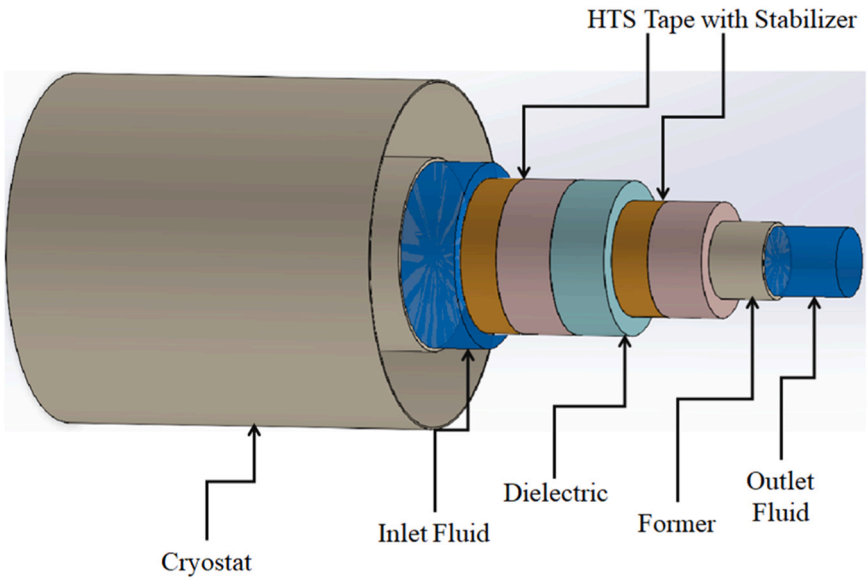

Fig. 2. A schematic of a bipolar DC HTS cableused for SBSP application.

$$N_e = \lceil \frac{I_{op}}{m \times I_c(T_{op})} \rceil \tag{3}$$

$$N_{g,i} = \lfloor \frac{P_f}{(\omega_{sc} + g)} \rfloor \tag{4}$$

where, N_e is the electrical number of HTS tapes, m is the design marginal factor, $I_c(T_{op})$ is critical current of HTS tapes at operating temperature of T_{op}, P_f is the perimeter previous layer, and $N_{g,i}$ is the number of tapes that could be laid on ith former. In Eq. (3), it is implicitly assumed, as a first approximation, that the magnetic field generated on the tapes by the transport current of the cable does not significantly affect the critical current, which is viable assumption due to the parallel orientation of the magnetic field and since in practical applications the magnitude does not exceed the tens of mT. It should be mentioned that unless, $N_{g,1} \geq N_e$, another HTS layer must be added to the cable structure.

Based on the opertional voltage of HTS cable, insulation thickness and its radius could be determined, as shown in Eqs. (5) and (6) (Stamm et al., 2020).

$$\delta_{ins} = \left(r_{f_i} + \delta_{sc_i}\right)\left(e^{\frac{V_{dc}}{\eta E_b\left(r_{f_i}+\delta_{sc_i}\right)}} - 1\right) \tag{5}$$

$$r_{ins_i} = \left(r_{f_i} + \delta_{sc_i}\right) + \delta_{ins} \tag{6}$$

where, E_b is breakdown voltage of selected insulation, δ_{ins} is thickness of selected insulation, and η is the safety factor which is in the range of 0.2–0.3 (Stamm et al., 2020).

Finally, and after designing all HTS layers of the cable, final radius of the cable core is calculated and then based on (Bruzek et al., 2014), the cryostat type is selected. Fig. 3 shows the design flowchart of the DC HTS cable to be used in SBSP application. As shown in this figure, the HTS

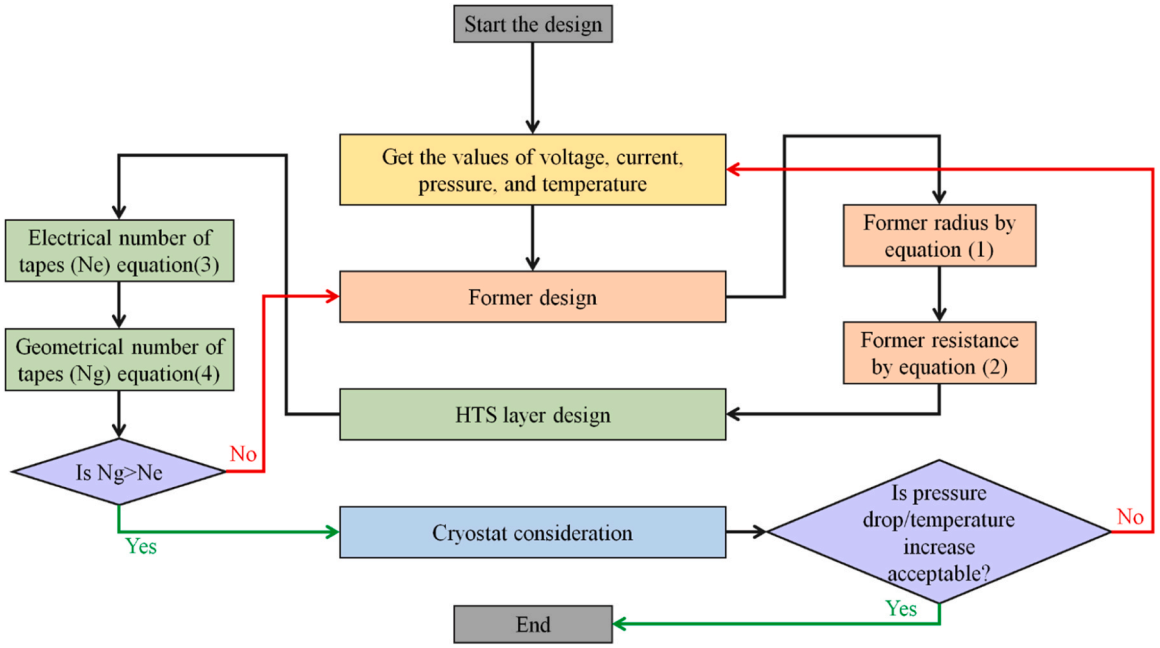

Fig. 3. Design flowchart of DC HTS cable.

cable design procedure starts with setting the operational electrothermal conditions, such as voltage, current, and temperature. Then, based on the previously discussed equations, the required electrical number of HTS tapes are calculated. Then, number of HTS tapes that are geometrically feasible on the perimeter of the former/previous HTS layer is calculated. if the total number of HTS tapes become bigger than electrical number of HTS tapes, the design procedure would go forward for cryostat calculations, unless another superconducting layer should be added, and the steps should be repeated. Finally, the design procedure would be finished after calculation related to the cryostats.

3. Modelling procedure

This section is dedicated to modelling procedure of DC HTS cables, based on their thermal, magnetic, and electrical characteristics.

3.1. Loss calculation in DC HTS cable

As shown in Eq. (7), total loss (Q_t) in any DC HTS cable – though extremely low compared with conventional copper cables – consists of multiple components. The first component $Q_{NL_{SC}}$is the loss originated in the superconductors, which is calculated according to Eq. (8) (Nolan et al., 2022). It should be mentioned that there are no ideal DC current/voltage waveforms without any ripples . Thus, voltage ripples impose a pseudo dielectric loss $Q_{vR}$to the cable while current ripples impose a pseudo-AC loss Q_{C_R}. These two ripple-based losses are calculated as shown in Eqs. (9) and (10) (Bruzek et al., 2014; Norris, 1970). There are also losses Q_{CL} that originate in the current leads, as shown in Eq. (11) (Glowacki et al., 2020). Finally, the loss generated by passing the current through the former layer is determined by using Eq. (12).

$$Q_t = L_C\left(Q_{NL_{SC}} + Q_{vR} + Q_{C_R} + Q_{Cry}\right) + 2\left(Q_{CL} + Q_{fo}\right) \tag{7}$$

$$Q_{NL_{SC}} = I_{op}^{n+1} E_c I_c^{-n}\left(T_{op}\right) \tag{8}$$

$$Q_{vR} = 2\pi f_R \tan\delta Cap_{cab} \Delta U^2 \tag{9}$$

$$Q_{C_R} = \frac{\mu_0 f_R}{\pi}\left[\left(I_c^2\left(T_{op}\right) - \frac{I_{RA} I_c\left(T_{op}\right)}{2}\right) \quad \ln\left(1 - \frac{I_{RA}}{I_c\left(T_{op}\right)}\right) + \left(I_c^2\left(T_{op}\right) I_{RA} - \frac{I_{RA}^2 I_c\left(T_{op}\right)}{4}\right)\right] \tag{10}$$

$$Q_{CL} = \quad I_{op}\sqrt{1600\rho_{cu}\left(T_{amb} - T_{op}\right)} \tag{11}$$

$$Q_{fo} = R_{fo} I_{fo}^2 \tag{12}$$

where, I_{op} is operating current, n is index value, E_c is critical electric field, f_R is ripple frequency, $\tan\delta$ is loss factor of insulation, Cap_{ins} is the capacitance value of the cable, ΔU is the half of full amplitude of voltage ripples at a given frequency, μ_0 is permeability of free space, I_{RA} is the ripple current amplitude, ρ_{cu} is resistivity of copper current leads, T_{amb} is ambient temperature, and I_{fo} is current passing through former.

After getting the total heat load values for DC HTS cables, Eqs. (13) and (14) could be used for determination of the required cooling power and mass of cooling system (Ladner, 2011). It should be noted that Eq. (13) is valid for temperature range of 5 K to 300 K and Eq. (14) is valid for the same temperature range and cooling power range of 0.1 W to 10 kW (Ladner, 2011).

$$P_{cooling} = \frac{1.1 Q_{tot} T_{amb} - 1.1 Q_{tot} T_{op}}{-3.5335 \times 10^{-9} \times T_{op}^4 - 9.9354 \times 10^{-6} T_{op}^3 + 3.2995 \times 10^{-3} T_{op}^2} \tag{13}$$

$$M_{cooling} = 0.62702 \times P_{cooling}^{0.5588} \tag{14}$$

where, $P_{cooling}$ is the cooling power, and $M_{cooling}$ is the mass of cooling system.

3.2. Temperature calculation of HTS cable

To calculate the temperature of ReBCO tapes, Eq. (15) could be used in steady-state where heat transfer between HTS layer and coolant fluid is assumed to be zero (Hahn and Özişik, 2012; de Sousa et al., 2021).

$$D_{ReBCO}(T) \quad C_{P_{ReBCO}}(T)\frac{\partial T}{\partial t} = k_{ReBCO}(T)\frac{\partial^2 T}{\partial r^2} + \frac{k_{ReBCO}}{r}\frac{\partial T}{\partial r} + Q_{tot} \tag{15}$$

where, $D_{ReBCO}(T)$ is the equivalent mass density of HTS tape, $C_{P_{ReBCO}}(T)$ is specific heat capacity of HTS tape, and $k_{ReBCO}(T)$ is thermal conductivity of ReBCO. It should be mentioned that, since thermal steady state is considered, radial conductive/convective heat transfer between different layers and longitudinal heat conduction are neglected (De Sousa et al., 2020), in Eq. (15).

3.3. Cost and weight calculation of HTS cable

In this section, weight and cost of different parts of an HTS cable are calculated. Eq. (16) is used to calculate the weight of former layers based on their radius (r_f), thickness (δ_f), and the density of the material used in the former layer (D_{fo}) (Sadeghi and Yazdani-Asrami, 2022). Then, Eq. (17) could be used to calculate the weight of HTS tapes in ith layer of the cable, where, α_i is the twisting angle in the ith layer of HTS cable and $N_{g\ i}$ is the number of tapes in ith layer (Musso et al., 2022a). The insulation weight and shield weight of the cooling system is calculated by using Eqs. (18) and (19) (Sadeghi and Yazdani-Asrami, 2022). Afterwards, based on the final designed value of cryostat layer radius (r_{cryo}), the weight of coolant fluid could be calculated by using Eq. (20), where D_{CF} is the density of the coolant fluid. Finally, the total weight of the cable is the summation of weights and the weight of cryostat (W_{cryo}) as shown in Eq. (21) which is discussed in detail in (Bruzek et al., 2014).

$$W_{fo} = \pi \quad L_C D_{fo}\left[\left(r_f + \delta_f\right)^2 - \left(r_f\right)^2\right] \tag{16}$$

$$W_{HTS_i} = \frac{2\pi r_{f_i}}{\omega_{sc}\cos(\alpha_i)} L_C \times N_{g\ \ i} \times D_{ReBCO} \tag{17}$$

$$W_{ins} = \pi \quad L_C D_{ins}\left[\left(r_{ins} + \delta_{ins}\right)^2 - \left(r_{ins}\right)^2\right] \tag{18}$$

$$W_{shield} = \pi \quad L_C D_{sh}\left[\left(r_{sh} + \delta_{sh}\right)^2 - \left(r_{sh}\right)^2\right] \tag{19}$$

$$W_{CF} = \pi \quad L_C D_{CF}\left[\left(r_{cryo}\right)^2 - \left(r_{ins} + \delta_{ins}\right)^2\right] \tag{20}$$

$$W_{tot} = W_{fo} + W_{HTS_{i,j}} + W_{ins} + W_{cryo} + W_{shield} + W_{CF} \tag{21}$$

After the calculation of weight for different layers of HTS cable, their

purchasing cost can be calculated. Firstly, Eq. (22) offers the cost of former layer based on the base cost of copper (cb_{fo}) in ($\frac{EUR}{kg}$) (Musso et al., 2022a). Then, the cost of superconducting tapes in HTS cable is calculated according to Eq. (23), where N_L is the number of HTS layers and cb_{HTS} is the base cost of HTS tapes in ($\frac{EUR}{m}$). Same as the former layer, insulation cost and shielding cost could be calculated according to Eqs. (24) and (25) (Lee et al., 2019; Politano et al., 2001). There are also other costs such as vacuum pump cost, cabling cost, termination cost, and laying/maintenance cost of HTS cables, that are shown in Eq. (26) (Musso et al., 2022a; Li et al., 2009). Finally, the total cost of HTS cable is the summation of the cost minus a discount value, shown in Eq. (27) (Musso et al., 2022a; Lee et al., 2016; Yuan et al., 2018), where *sy* is the service year of the cable, Φ and is the discount percentage.

$$C_{fo} = W_{fo} \times cb_{fo} \tag{22}$$

$$C_{HTS_{i,j}} = \sum_{i=1}^{N_L} L_{HTS_i} \times N_{g\ \ i} \times cb_{HTS} \tag{23}$$

$$C_{ins} = W_{ins} \times cb_{ins} \tag{24}$$

$$C_{shield} = W_{shield} \times cb_{sh} \tag{25}$$

$$C_{other} = C_{vac} + C_{cab} + C_{term} + C_{lay} \tag{26}$$

$$C_{tot} = (C_{fo} + C_{HTS_{i,j}} + C_{ins} + C_{cryo} + C_{shield} + C_{other}) - \left(\sum_{i}^{sy} \frac{L_C \times C_{man}}{sy(1+\Phi)^i} + \frac{C_{dis}}{(1+\Phi)^{sy}} \right) \tag{27}$$

where, C_{cryo} is the cryostat cost, C_{man} is the maintenance cost, and C_{dis} is the dismantling cost. It should be mentioned that in this study, also the cost of the manufacturing of HTS cables is assumed to be as 20–25% of the cost of the materials used for HTS cable, based on the study presented in (Morandi et al., 2016).

4. Results and discussions

In this section, firstly, the power system of SBSP where the HTS cable is implemented, will be explained, then, based on the voltage, current, and ripple characteristics of this grid, the design of the HTS cable will be discussed.

4.1. Power grid of the SBSP

Fig. 4 shows the internal electric power system of a SBSP, according to (Powell et al., 2002), where solar panels receive the energy of the sun and turn them into DC electric energy. After that, DC/DC converters are used to reduce the voltage level of harvested sun energy to 80 volts and increase its current to 12.5 kA. Then, two poles of HTS cables are used to transmit the power with high current low voltage characteristics. The low voltage characteristic is preferred to reduce the thickness of electrical insulation (Yazdani-Asrami et al., 2022a), and dielectric loss, without significantly impacting the cable size. Finally, another DC/DC converter unit is used to increase the voltage level of electricity and transmit the power to the RF generators. In this level, electrical power is converted into microwaves/lasers and beamed to the Earth. In this structure, and due to the implementation of HTS cables, a cryogenic cooling system and a coolant tank are required to maintain the superconducting state of the HTS cable.

4.2. Design of DC HTS cable for SBSP application

The characteristic of HTS tapes varies considering temperature changes, therefore, four operating temperatures have been considered for DC HTS cable design, namely, 20 K, 30 K, 50 K, 65 K and 77 K. These are the operating temperatures can be reached by employing Liquid Hydrogen (LH_2), Gaseous Helium (GHe), and Liquid Nitrogen (LN_2) as the most probable cryogenic coolant fluids to cool down the HTS devices in aerospace application, as stated in (Yazdani Asrami et al., 2022; Radebaugh, 2004). The logic behind the selection of these temperatures

Table 1
Specifications of HTS tapes used to design the HTS cable for the SBSP application (Anon Robinson HTS Wire Critical Current Data Base).

Parameter	Value	Unit
Ic @65 K & 0 T	338	*A*
Index value @65 K & 0 T	23.43	-
Width	12	*mm*
Thickness	160	*μm*
Substrate thickness (Hastelloy)	100	*μm*
Copper stabiliser thickness	50	*μm*
ReBCO thickness	3	*μm*
Silver shield thickness	1.6	*μm*
MgO layer thickness	3.3	*μm*

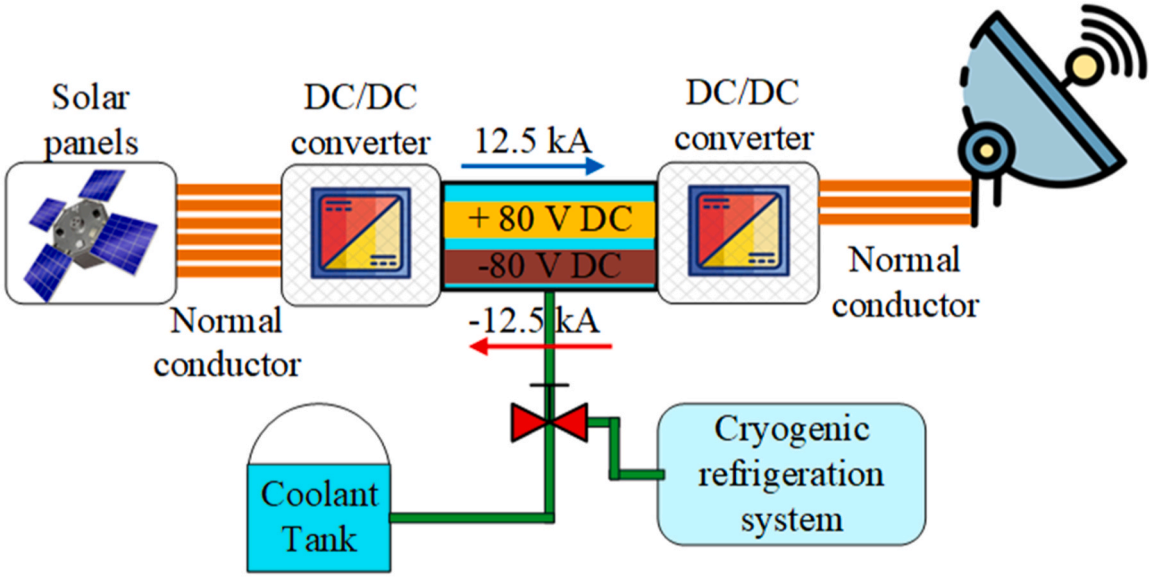

Fig. 4. Internal power system of a SBSP system with DC HTS cable implemented in it.

is to analyse the impact of different coolant fluids on the final weight and cost of cable, minimum loss in DC cables, final cost of coolant fluid, and peak temperature of HTS cable. To minimize the number of superconductors required, under each operating temperature, an HTS tape manufactured by THEVA is selected that has an high critical current even at 77 K temperature (Anon Robinson HTS Wire Critical Current Data Base). The most important specifications and properties of the selected HTS tape are tabulated in Table 1. It should be noted that based on (Bruzek et al., 2014), coaxial structure is the most efficient structure of DC HTS cable for voltages lower than 20 kV. This cable is highly compact and common terminations and joints could be used for both poles. It should be noted that the critical and index value of the HTS tape is reported in Table 1 at 65 K temperature, however, to design the HTS cable in other temperatures, critical current values should be adjusted. The critical current values for temperatures of 20 K, 30 K, 50 K, and 77 K are 978 A, 832 A, 545 A, and 162 A, respectively. The index values also at these temperatures are 36.2, 25.5, 23.8, and 21.5, respectively (Anon Robinson HTS Wire Critical Current Data Base).

Table 2 summarizes different parameters of the HTS cable under each considered operational temperature. At this stage, three different fluids have been considered as cryogenic coolant fluids of the HTS cable, Due to different critical currents at different operational temperatures, the number of HTS layers increases concerning operational current increase. Based on these changes, the final critical current of the HTS cable, the final radius of the HTS cable, etc. have been changed. Table 3 shows all the parameters that have been used for weight and cost calculation of the designed HTS cables.

4.3. Loss and temperature comparison of different cable designs

Fig. 5 displays the maximum value of total losses per unit length in each designed HTS cable. The lower operational temperature results in higher critical currents and thus, the magnitude of the total loss would be lower. The higher losses in HTS cables with operational temperatures of 50 K to 77 K are mainly due to the higher number of superconducting layers and reduction of the critical current. For instance, when the number of superconducting layers increases to 7 for cable with operational temperature of 50 K, the total loss of the cable would increase by 31% and when the number of layers increases to 9, the total loss would increase 44%.

This shows how the number of superconducting layers could affect the maximum heat load injected to the cooling system. Fig. 6 shows how the calculated losses affect the maximum temperature in designed cables. Here, the figure is normalized based on the operational temperature to help the readers in understanding the impact of heat loads at different temperatures. The lower the operational temperature gets, the lower the heat capacity of ReBCO tapes are. Thus, lower heat could increase their temperature more, compared to higher operating temperatures. As an example of this, the heat load in 20 K is about 31% lower than the heat load in 77 K while the maximum temperature of the cable is about 14% higher than cable operating in 77 K temperature. It should be noted that the results of Figs. 5 and 6, are calculated for 0.1% of ripple amplitude and at 50 Hz. Fig. 7 illustrates the cooling system power and mass of DC HTS cables scenarios operating in different operational temperatures. The required cooling power at room temperature of DC HTS cable in 20 K is about 3.2 kW while this value for HTS cable of 77 K is about 400 W. Just consider that heat load of DC HTS cable in 20 K is about 32% lower than heat load of DC HTS cable at 77 K.

Table 2
Final HTS cable sizing parameters based on different operating temperatures.

Operating temperature	20 K	30 K	50 K	65 K	77 K
Probable coolant fluid	LH_2	GHe	GHe	LN_2	LN_2
D_{CF} $\left(\frac{kg}{m^3}\right)$ Yazdani-Asrami et al., (2022b)	70.8	178	178	807	807
Number of HTS layers in the positive pole	2	3	4	6	12
Number of HTS layers in the negative pole	2	3	4	6	11
Total number of HTS tapes in the positive pole	21	32	43	65	131
Total number of HTS tapes in the negative pole	22	33	44	66	134
The radius of the insulation in positive pole (mm)	21.82	21.98	22.14	22.46	23.42
Radius of the insulation in negative pole (mm)	22.64	22.96	23.28	23.92	25.68
Radius of shield layer	23.64	23.96	24.28	24.92	26.68

Table 3
Weight, cost, and magnetic parameters used to model the HTS cable for SBSP application (Musso et al., 2022b).

Parameter	Value	Unit
δ_f	1	mm
δ_{ins}	0.5	mm
$\tan\delta$	0.001	–
D_{ins}	910	$\frac{kg}{m^3}$
D_{fo}	8960	$\frac{kg}{m^3}$
D_{sh}	8960	$\frac{kg}{m^3}$
cb_{fo}	8.14	$\frac{EUR}{kg}$
cb_{HTS}	35	$\frac{EUR}{m}$
cb_{ins}	10	$\frac{EUR}{m}$
cb_{sh}	8.14	$\frac{EUR}{m}$
c_{cryo}	100	$\frac{EUR}{W}$
C_{vac}	52	$\frac{EUR}{m}$
C_{cab}	3	$\frac{k.EUR}{m}$
C_{term}	60	$\frac{EUR}{m}$
C_{lay}	20	$\frac{k.EUR}{m}$
C_{dis}	20	$k.EUR$
C_{man}	10	$k.EUR$
sy	50	$year$
Φ	0.1	-

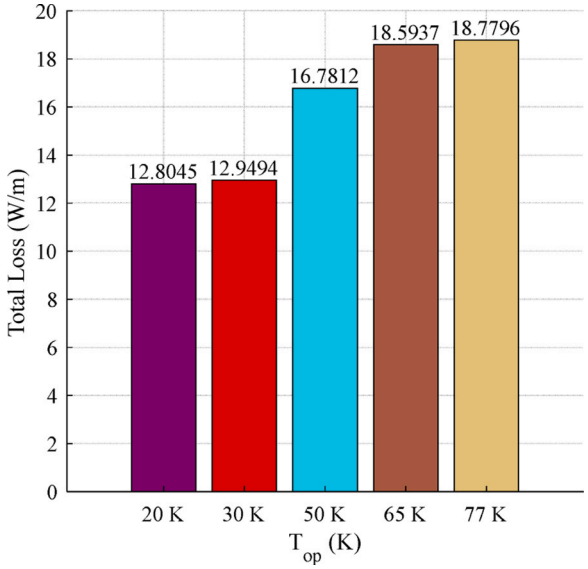

Fig. 5. Total loss of designed HTS cables with respect to different temperature.

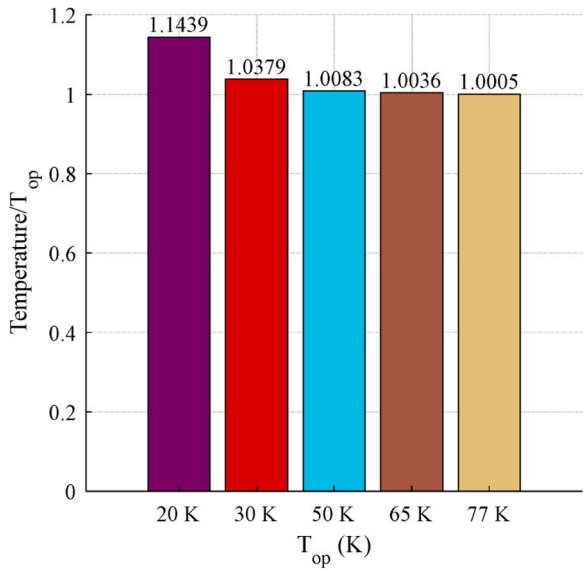

Fig. 6. Temperature of designed HTS cables with respect to different temperature.

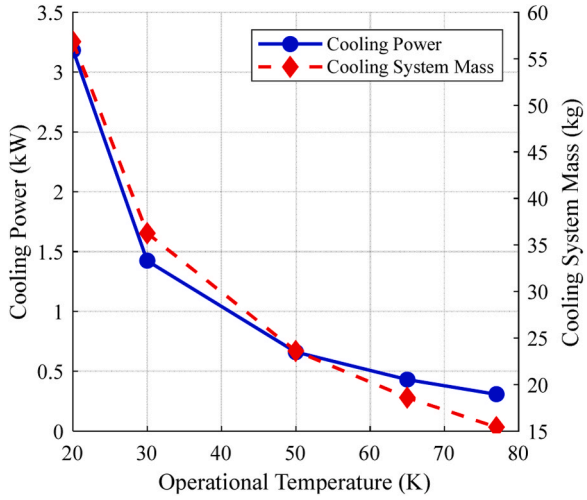

Fig. 7. Required cooling power and cooling system mass of designed HTS cables with respect to different temperature.

Considering these two values of cooling power and heat load, it could be conceived that the application of DC HTS cables in 77 K temperature is more rational in terms of cooling system power. The next item about cooling system is considering the mass of cooling systems. In this regard, mass of cooling system at 77 K is about 15 kg while the mass of DC HTS cable at 20 K (with lower heat load) is about 56 kg, for a 1 meter DC HTS cable. This means that cooling system mass decreases with the operational temperature increase. For space applications, DC HTS cables that operate in higher temperatures are more beneficial in terms of cooling system mass and required power.

Fig. 8 illustrates the impact of ripple characteristics on the total loss of the designed HTS cables in 20 K, 30 K, 50 K, 65 K and 77 K, respectively. As seen in this figure, the higher the ripple frequency gets, the total losses increase. This is also the case for increasing the ripple amplitude. For instance, in 20 K, when, ripple amplitude is 0.1% for 50 Hz ripple frequency, total loss is about 12.8 W/m while this number for 10% ripple amplitude and 10 kHz frequency is about 15.8 W/m (about 23% increase). The loss increase rate versus ripple characteristic is about 31% in 30 K, about 33% in 50 K, and about 21% in 65 K. This high level of losses in high ripple frequencies and amplitudes shows the importance of designing the power converters so that the maximum heat load imposed to cooling systems are reduced.

4.4. Cost comparison of different cryostat cable designs

In this section and based on parameters presented in Table 3, cost and weight of different components of HTS cables are analysed per unit length and then listed in Table 4. Due to the increase in number of the superconducting layers with respect to the operational temperature increase, the weight and the cost would be increased. The cost of HTS cable for 65 K is about 167% higher compared to 20 K and 30 K designs, this value for 77 K is 303%. This value for weight is also about 167%. Copper has higher density and lower per unit length price, compared to HTS tape. As a result of this, the weight of copper former is higher than HTS tapes weight while the purchasing cost of copper former is about 38 times lower than HTS tapes purchasing cost. Afterwards, minimum efficiency of the cable is calculated based on the highest total loss which is in 10% ripple amplitude and 10 kHz ripple frequency. As can be seen from Table 4, due to the higher number of HTS layers at 65 K, the total weight of HTS cable is about 144% higher while its cost is about 170% higher. About HTS cable in 50 K, its weight is 82% higher than 20 K cable and 25% lower than 65 K cable, these numbers for cost are 94% and 40%.

4.5. Recommendations for manufacturing SSP-specific superconductors

As seen in previous sections, at higher operating temperatures, the number of HTS tapes and superconducting layers increases. However, higher cryogenic temperature is much more practical for space applications because cryogenic cooling systems get heavier, more expensive, with base operating temperature reduction. In addition, cryocoolers need higher power at lower temperatures which would be struggle to provide it in space missions. The loss generated by HTS tapes is another problem that should be considered by manufacturers where an HTS tape with higher engineering current is needed that could end up with lower losses in HTS tapes and higher efficiency of HTS cable. This is not only important from cable performance and efficiency point of view, but also quite critical as higher loss requires higher cooling power. Thus, providing such higher cooling power would not be easy in space. Another important fact about the HTS tapes is that they face some structural fractures during their manufacturing processes. These microfractures could increase the probability of quenches and weak points that can be quite catastrophic in a space mission. Artificial Intelligence (AI) techniques could play a vital role by acting as a supervisor during the whole process of HTS tape manufacturing and manage this process so that the microfracture number minimized (Yazdani-Asrami et al., 2023, 2022c; Yazdani-Asrami, 2023).

Finally, it should be mentioned that there is a trade-off between the cooling cost of the cable and the cost of superconducting tapes that is used in HTS cable. By the increasing the temperature from 20 K to 77 K, the cost of superconducting tapes would be approximately 200% increased while the cost of the cooling system would be 67% reduced. However, one should remind that the cost of superconducting tapes is in range of thousands of euros while the range of cooling system is in millions of euros. This means that by increasing the temperature from 20 K to 77 K, about 2.1 million euros would be saved, without considering the impact of temperature on energy loss. On the other hand, by reducing the temperature from 77 K to 20 K, although HTS tapes could save us about 5.68 thousand of euro, the cooling system would impose 2.15 million euros more to the cost of cooling system. Thus, during the design of the HTS cable for SBSP applications, these considerations must be considered.

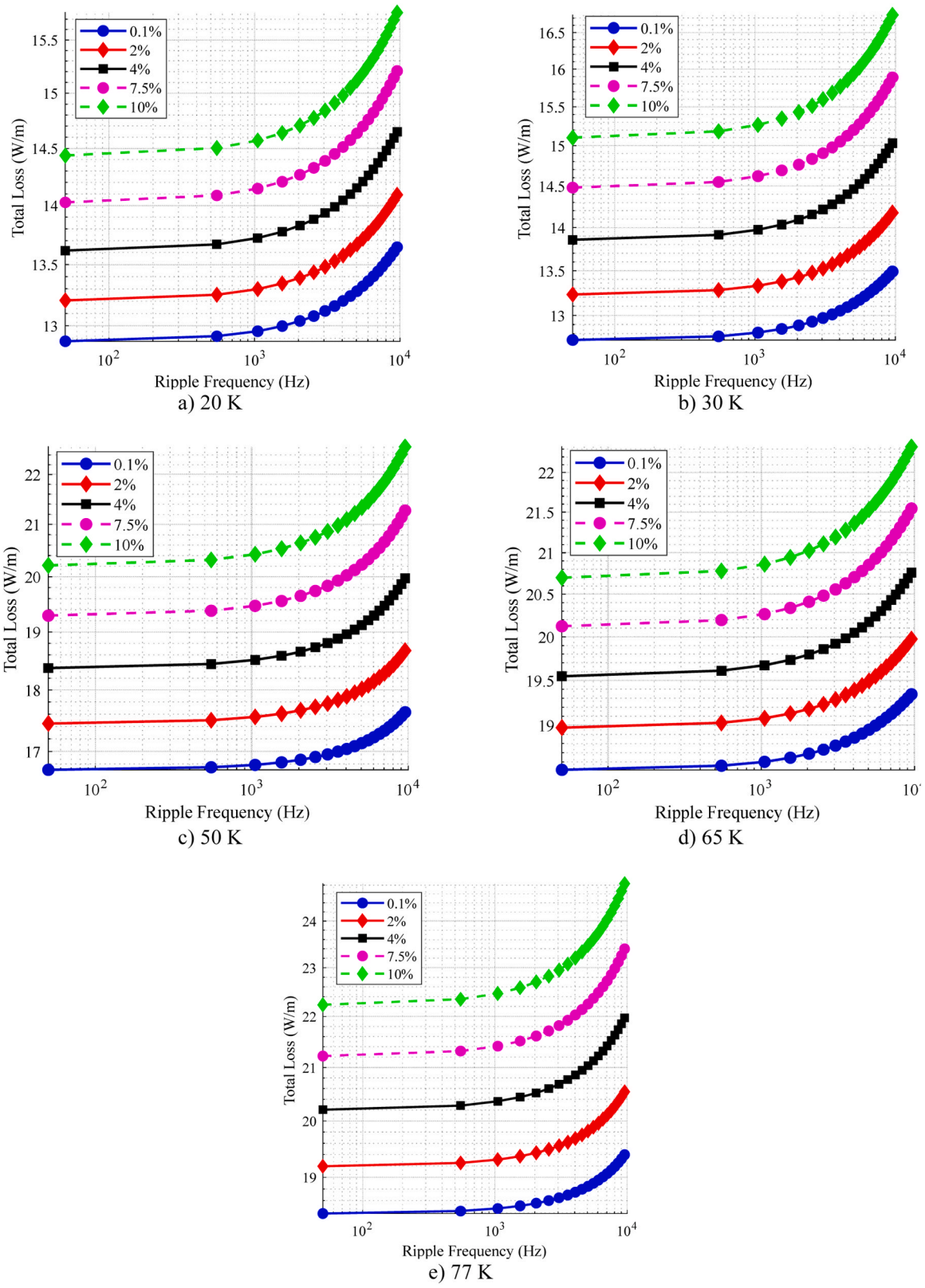

Fig. 8. Total loss of designed HTS cables with respect to changes of ripple frequency at different operational temperatures and for different ripples' amplitudes.

4.6. Comparing to conventional XLPE power cables

The aim of this section is to compare the weight and energy loss of a conventional power cable with those of HTS cables, in SBSP applications. For this purpose, two conventional cables have been considered, one with copper core and the other with aluminium core. Eq. (25) is used to design the conventional cables based on the operational current I_{op}, cable length L_c, conductivity of cable core K_{core}, maximum allowable voltage drops ΔU_c, and operating DC voltage of the system U_{DC}. Eq. (26) is also used to calculate the core weight of conventional cables with

Table 4
Weights and costs of designed HTS cables with respect to changes of operating temperatures.

Operational temperature	20 K	30 K	50 K	65 K	77 K
Weight & Cost of HTS tapes (kg/m & *EUR* /m)	2.59 & 436.66	3.92 & 656.87	5.25 & 886.29	7.91 & 1350.11	8.27 & 2686.01
Weight & Cost of former (kg/m & *EUR* /m)	1.15 & 9.39	1.15 & 9.39	1.15 & 9.39	1.15 & 9.39	1.15 & 9.39
Weight & Cost of insulations (kg/m & *EUR* /m)	0.125 & 0.09	0.127 & 0.1	0.128 & 0.11	0.131 & 0.12	0.139 & 0.15
Weight & Cost of shielding layer (kg/m & *EUR*/m)	1.30 & 10.61	1.32 & 10.75	1.34 & 10.89	1.37 & 11.19	1.47 & 11.99
Other costs (*EUR*)	2311	2311	2311	2311	2311
Manufacturing cost (*EUR* /m)	114.17	170.06	226.64	342.35	676.85
Cable efficiency (%), no cooling system	99.9992	99.9991	99.9989	99.9988	99.9987
Required cooling power (kW)	5.88	2.61	0.93	0.55	0.39
Cable efficiency (%), with cooling system	99.7052	99.8690	99.9524	99.9715	99.9794
Total weight and total cost per unit length (kg/m & k *EUR* /m) (no cooling system)	9.25 & 2.88	10.59 & 2.99	11.94 & 3.44	14.63 & 4.02	22.79 & 5.69
Cost of cooling system (M EUR/m)	2.82	2.02	1.28	1.02	0.671

Table 5
Electro-physical parameters of conventional power cables.

Cable type	Copper core	Aluminium core
Electrical conductivity (S/m)	5.95×10^7	3.77×10^7
Cable length (m)	10–200	10–200
Density (kg/m^3)	8960	2700

respect to the density of core material D_{core}. Finally, the Eq. (27) is used to calculate the core loss in conventional cables (Gonen, 2009).

$$S_{core} = \frac{2I_{op} \quad L_c}{K_{core}\Delta U_c \quad U_{DC}} \tag{25}$$

$$W_{core} = S_{conv} \quad L_c \quad D_{core} \tag{26}$$

$$Q_{core} = \frac{L_c I_{op}^2}{K_{core} S_{core}} \tag{27}$$

Table 5 tabulates the electrical and physical parameters used to calculate the weight and loss of conventional power cables in this paper.

Fig. 9 shows the weight of different HTS cables compared to the weight of conventional power cables, under 12.5 kA nominal current, 80 V DC voltage. The same voltage is assumed for both the superconducting and the convention cable, so must have the same power electronic converters for both the systems. The low voltage value considered for copper cables as well as HTS cables is based on output voltage of the power electronic units that convert the solar energy to electrical energy. It should be considered that increasing the voltage needs either heavier and more expensive power electronic converters which will increase both launching cost of the spacecraft as well as the weight of whole system. As seen in this figure, the maximum weight of the core of HTS cables is between 1 and 3 tons which is about 96–99% lighter than the weight of conventional copper and aluminium power cables. These differences in core weight of HTS cables compared to conventional ones, could impact the total weight of satellite, amount of required propulsion needed by satellite, and the total efficiency of the SBSP system.

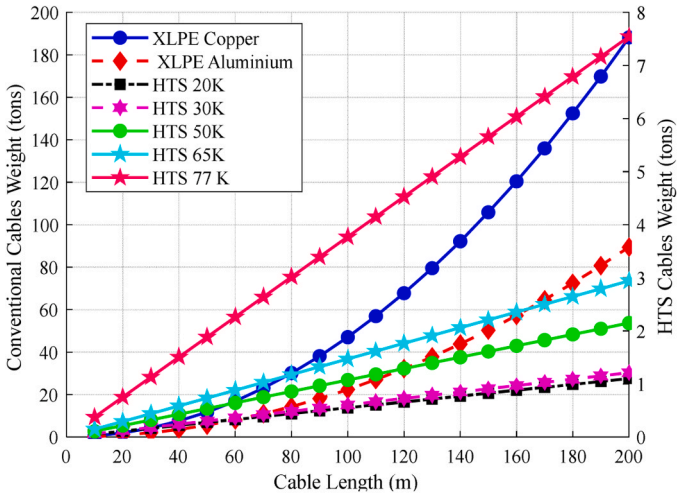

Fig. 9. The weight comparison of HTS cables versus conventional cables.

To discuss the impact of using conventional power cables on the total efficiency of the SBSP system, Fig. 10 is presented that shows the total power loss in conventional and HTS cables with respect to changes in cable length. The Joule heat loss in conventional cables that is just related to core loss, is in range of MW values while the total loss of HTS cable, including all components of loss, is in kW range. For instance, the loss of HTS cable in 77 K and cable length of 200 m is about 4.7 kW while the loss of a 20 m copper cable is about 700 kW and for aluminium cable is about 900 kW. This means that a 200 m HTS cable operating at 77 K (as the heaviest HTS cable with highest loss value), generates about 99% less loss compared to copper counterpart in 10x shorter length. If one compares the 10 m length for 65 K HTS cable with 10 m conventional cables, would observe that the loss in conventional cables is about 1250x higher than HTS cables at 77 K. The large amount of dissipated power by conventional cables, could impact the economic and thermal considerations related to the SBSP projects.

Fig. 10 shows the dissipated power loss of HTS cables and conventional cables at different cable lengths. In Fig. 10(a), the power loss in HTS cables, without considering the cooling system, is presented. The 77 K HTS cable exhibits the highest power loss, reaching around 4.8 kW at a length of 200 m, while the values for the 65 K and 50 K HTS cables are approximately 4.5 kW. Additionally, the 77 K HTS cable has about 35% higher dissipated power than the 20 K and 30 K HTS cables. In Fig. 10(b), the impact of the cooling system is considered. The dissipated power for 20 K and 30 K HTS cables increases abruptly due to the higher power requirement for extracting 1 W heat load out of the cryostat at 20 K/30 K temperatures compared to 65 K or 77 K temperatures. For a 200-meter length of 20 K HTS cable, the efficiency is reduced to approximately 50%, which is impractical for SBSP applications. However, even with the cooling system considered for 65 K and 77 K HTS cables, the efficiency remains well above 98%. It's important to note, as shown in Fig. 10(c), that using copper and aluminium cables for lengths exceeding 40 m is not feasible. This is because at higher lengths, the power loss surpasses the total power transmitted by the cable.

Fig. 11(a) shows the annual energy loss of the conventional aluminium and copper cables to transmit the energy harvested by SBSP. In this manner, the amount of energy loss during one year for copper cable is about160 TJ and for aluminium cable is about 255 TJ. On the other hand, Fig. 11(b) shows the annual energy loss of the HTS cables by neglecting the power required by cooling system. In this case, the 77 K HTS cable has highest energy loss which is 100x lower than energy loss by copper cable, while this number for 20 K HTS cable is 150x lower than copper cable. As shown in Fig. 11(c), by considering the impact of cooling system on energy loss, 20 K HTS cable would have highest

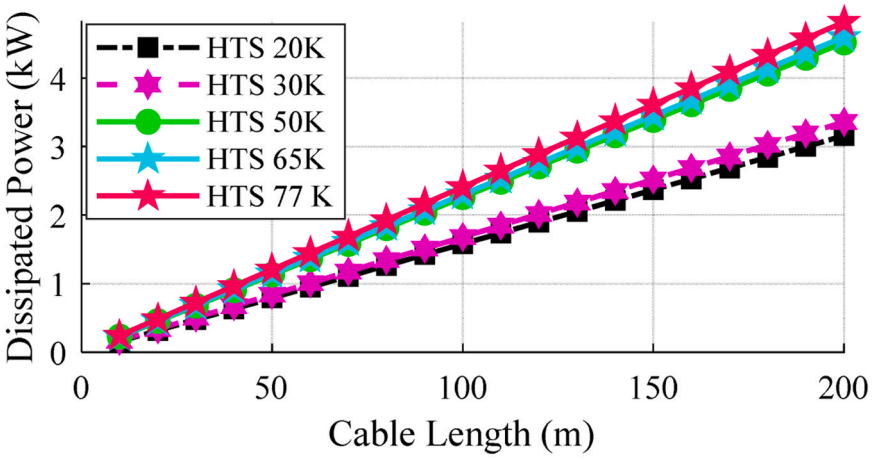

a) Dissipated power in HTS cables without considering cooling system

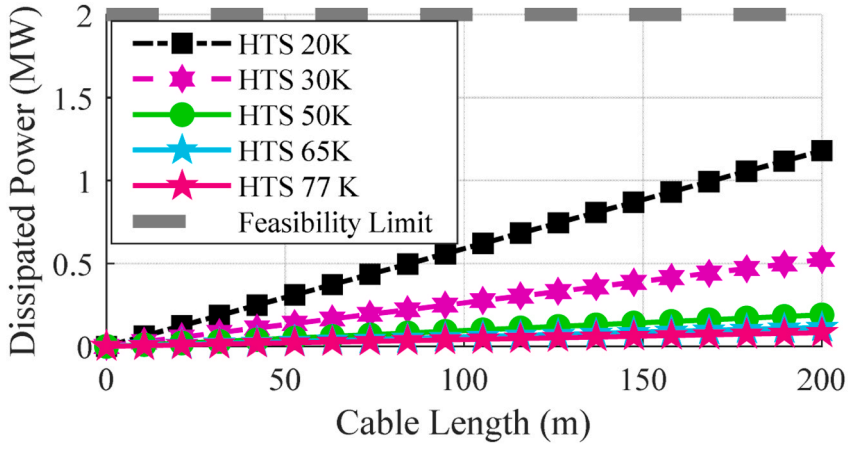

b) Dissipated power in HTS cables by considering cooling system

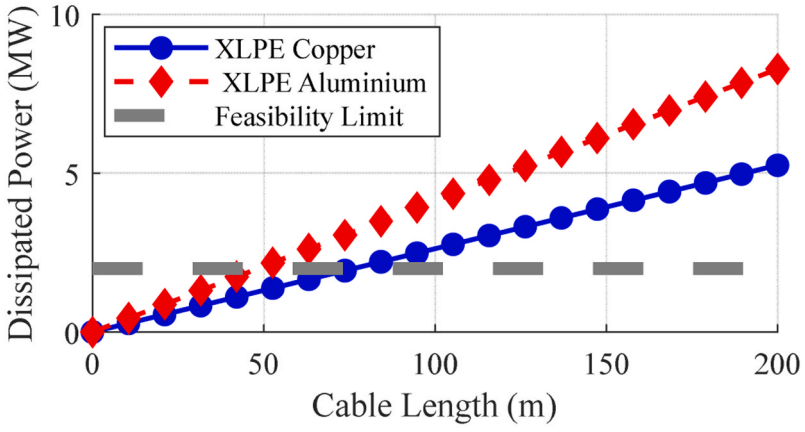

c) Dissipated power in conventional cables

Fig. 10. The loss comparison of HTS cables versus conventional power cables.

energy loss which is about 50 TJ. However, in this case, 20 K HTS cable still outperforms the copper and aluminium cable, in terms of annual energy loss. In this case, the annual loss of the 20 K HTS cable is still 3x lower than copper cable. By considering the cooling and HTS cable energy loss for 77 K temperature, it would be observed that the 77 K HTS cable has still approximately 50x lower annual loss. As a result of this, the conventional cables are infeasible for such high current and low voltage characteristic of the SBSPs.

It should be noted that a full optimization procedure could be considered as the next steps for this study, where objective function could be either minimization of total ownership cost of HTS cable or maximizing the energy harvested of the SBSP satellite. However, for such optimization, a system-level analysis is needed that considers the cost of the power electronic devices and RF generators, as well as the efficiency of them, like the studies conducted in (Burkart and Kolar, 2017; Domingues-Olavarria et al., 2017; Burkart and Kolar, 2013; Ives

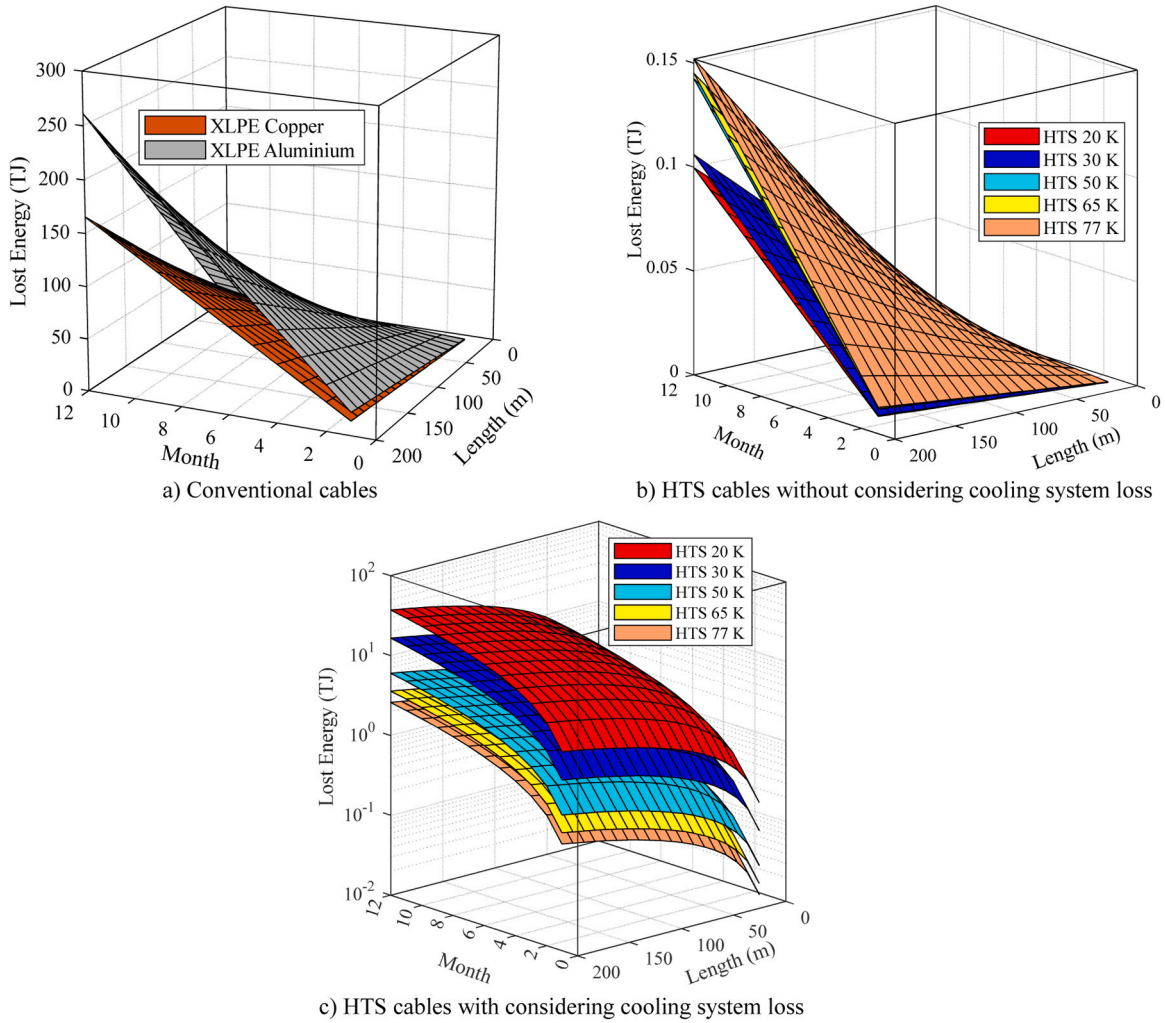

Fig. 11. The value of energy loss for one-month operation of SBSP, a) conventional power cables, b) HTS cables.

et al., 2023; Paz et al., 2019) for terrestrial applications.

5. Conclusion

This paper has presented an analysis of the design and feasibility of employing High Temperature Superconducting (HTS) cables for Space Solar Power Satellite (SBSP) applications. The presented study investigated the performance of DC HTS cables at various operational temperatures (20 K, 30 K, 50 K, 65 K, and 77 K), focusing on their cost, weight, and magneto-thermal constraints. Key findings indicate that higher operational temperatures significantly reduce the loss and cost of HTS cables, with the 65 K and 77 K designs being notably more advantageous in terms of efficiency and cost-effectiveness. Moreover, we demonstrated that employing HTS technology in SBSP could dramatically reduce energy losses compared to conventional copper or aluminium cables, highlighting the potential for substantial efficiency improvements in space-based energy transmission systems. For example, the heat load in 20 K is about 31% lower than the heat load in 77 K while the maximum temperature of the cable is about 14% higher than cable operating in 77 K temperature. The cost of HTS cable for 77 K is about 167% higher compared to 20 K and 30 K designs. Due to the higher number of HTS layers at 77 K, the total weight of HTS cable is about 144% higher while its cost is about 170% higher than cable in 20 K. The required cooling power for 77 K DC HTS cable is 32% lower than the HTS cable in 20 K. The mass of cooling system for DC HTS cable operating at 77 K is 74% lower than DC HTS cable operating in 20 K. For HTS cable in 50 K, its weight is 82% higher than 20 K cable and 25% lower than 77 K cable, these numbers for cost are 94% and 40%. By considering only weight/cost of HTS cable components, HTS cable in 20 K and 30 K is much more beneficial for solar satellite, however, the impact of cooling system must be considered. In SBSP, using a copper or aluminium cable results in 160 TJ to 260 T energy loss per year which is approximately equal to energy consumption of United Kingdom in 2022. By using HTS technology in temperature ranges from 20 K to 77 K, the amount of energy loss would be 0.1 TJ to 0.15 TJ which means more than thousands of times reduction. This research underlines the critical role of operational temperature in optimizing HTS cable designs for SBSP applications, offering insights into their practical implementation and suggesting a path toward more sustainable and efficient energy harvesting from space. The next steps of this study would be fault performance analysis of designed HTS cables and optimization of the HTS cables, based on the different objective functions.

CRediT authorship contribution statement

Alireza Sadeghi: Writing – original draft, Visualization, Software, Methodology, Investigation, Formal analysis, Data curation. **Mohammad Yazdani-Asrami:** Writing – review & editing, Writing – original draft, Validation, Conceptualization, Formal analysis, Funding acquisition, Investigation, Methodology, Project administration, Resources, Supervision. **Antonio Morandi:** Writing – review & editing, Validation, Supervision, Investigation, Formal analysis.

Declaration of Competing Interest

The authors declare that they have no known competing financial interests or personal relationships that could have appeared to influence the work reported in this paper.

Data availability

No data was used for the research described in the article.

Acknowledgments

This work was supported by the U.K. Engineering and Physical Sciences Research Council (EPSRC) under Grant EP/X5257161/1.

References

Yazdani-Asrami, M., Seyyedbarzegar, S.M., Sadeghi, A., Sousa, W.T.B. de, Kottonau, D., 2022a. High temperature superconducting cables and their performance against short circuit faults: current development, challenges, solutions. Future Trends Supercond. Sci. Technol. 35, 083002.

Morandi, A., 2015a. HTS dc transmission and distribution: concepts, applications and benefits. Supercond. Sci. Technol. 28, 123001.

Sytnikov, V.E., Bemert, S.E., Krivetsky, I.V., Karpov, V.N., Romashov, M.A., Shakarian, Y. G., Nosov, A.A., Fetisov, S.S., 2016. The Test Results of AC and DC HTS Cables in Russia. IEEE Trans. Appl. Supercond. 26.

Sadeghi, A., Seyyedbarzegar, S.M., Yazdani-Asrami, M., 2021. Transient analysis of a 22.9 kV/2 kA HTS cable under short circuit using equivalent circuit model considering different fault parameters. Phys. C: Supercond. Appl. 589, 1353935.

Klöppel, S., Marian, A., Haberstroh, C., Bruzek, C.E., 2021. Thermo-hydraulic and economic aspects of long-length high-power MgB2 superconducting cables. Cryog. (Guildf.) 113.

Sadeghi, A., Seyyedbarzegar, S., Yazdani-Asrami, M., 2022. Investigation on the Electrothermal Performance of a High-Temperature Superconducting Cable in an Offshore Wind Farm Integrated Power System: Fault and Islanding Conditions. IEEE Trans. Appl. Supercond. 32, 1–11.

Sadeghi, A., Yazdani-Asrami, M., 2022. Multi-objective optimization for improvingweight and fault characteristics of a DC HTS cable in cryo-electric aircraft. Aerospace 9, 753.

Yazdani-Asrami, M., Song, W., Morandi, A., De Carne, G., Murta-Pina, J., Pronto, A., Oliveira, R., Grilli, F., Pardo, E., Parizh, M., Shen, B., Coombs, T., Salmi, T., Wu, D., Coatanea, E., Moseley, D.A., Badcock, R.A., Zhang, M., Marinozzi, V., Tran, N., Wielgosz, M., Skoczeń, A., Tzelepis, D., Meliopoulos, S., Vilhena, N., Sotelo, G., Jiang, Z., Große, V., Bagni, T., Mauro, D., Senatore, C., Mankevich, A., Amelichev, V., Samoilenkov, S., Yoon, T.L., Wang, Y., Camata, R.P., Chen, C.-C., Madureira, A.M., Abraham, A., 2023. Roadmap on artificial intelligence and big data techniques for superconductivity. Supercond. Sci. Technol. 36, 043501.

Marchionini, B.G., Yamada, Y., Martini, L., Ohsaki, H., 2017. High-Temperature Superconductivity: A Roadmap for Electric Power Sector Applications, 2015–2030. IEEE Trans. Appl. Supercond. 27, 1–7.

Cheetham, P., Ravindra, H., Stamm, T., Park, C., Kim, C., Graber, L., Steurer, M., Pamidi, S., 2019. High Temperature Superconducting Power Cables for MVDC Power Systems of Navy Ships. IEEE Electr. Ship Technol. Symp. . (ESTS) *2019*, 548–555.

Vorreiter, J.W., 1980. Cryogenic systems for spacecraft. Conte Phys. 21, 201–217.

Kervendal, E.A., Kirk, D.R., Meinke, R.B., 2009. Spacecraft Radiation Shielding Using Ultralightweight Superconducting Magnets. J. Space Rockets 46, 982–988.

Bergen, A., van Weers, H.J., Bruineman, C., Dhallé, M.M.J., Krooshoop, H.J.G., ter Brake, H.J.M., Ravensberg, K., Jackson, B.D., Wafelbakker, C.K., 2016. Design and validation of a large-format transition edge sensor array magnetic shielding system for space application. Rev. Sci. Instrum. 87.

Chesny, D.L., Levin, G.A., Persons, L.E., Durrance, S.T., 2020. Galactic Cosmic Ray Shielding Using Spherical Field-Reversed Array of Superconducting Coils. J. Space Rockets 57, 1222–1231.

Calvelli, V., Dilasser, G., Maksoud, W.A., Berriaud, C., Juster, F.-P., Lottin, J., Madur, A., Nunio, F., Rifflet, J.-M., Scola, L., 2020. 2D and 3D Conceptual Magnetic Design of the MADMAX Dipole. IEEE Trans. Appl. Supercond. 30, 1–5.

Ma, Z., Wang, Q., Wu, Z., Chen, D., Yan, C., Shi, Y., Dickey, M.D., Su, B., 2022. A Superconducting-Material-Based Maglev Generator Used for Outer-Space. Adv. Mater. 34.

Yang, W., Ji, Y., Yu, L., Liu, X., Long, J., Liu, Z., Song, D., 2020. Low frequency rotational loss in a high-temperature superconducting bearing and its application in micro-thrust measurement for space propulsion. Supercond. Sci. Technol. 33, 014001.

Cassady L., Chancery J., Squire J., Chang-Diaz F., Longmier B., Carter M., Glover T., McCaskill G., Olsen C. and Bering E. 2009 VASIMR Technological Advances and First Stage Performance Results *45th AIAA/ASME/SAE/ASEE Joint Propulsion Conference & Exhibit* (Reston, Virigina: American Institute of Aeronautics and Astronautics).

Matsumura, T., Kataza, H., Utsunomiya, S., Yamamoto, R., Hazumi, M., Katayama, N., 2016. Design and Performance of a Prototype Polarization Modulator Rotational System for Use in Space Using a Superconducting Magnetic Bearing. IEEE Trans. Appl. Supercond. 26, 1–4.

Jiqiang, Tang, Jiancheng, Fang, Wen, Wen, 2012. Superconducting Magnetic Bearings and Active Magnetic Bearings in Attitude Control and Energy Storage Flywheel for Spacecraft. IEEE Trans. Appl. Supercond. 22, 5702109–5702109.

Groll, M., 2023. Can climate change be avoided? Vision of a hydrogen-electricity energy economy. Energy 264, 126029.

Kamani, D., Ardehali, M.M., 2023. Long-term forecast of electrical energy consumption with considerations for solar and wind energy sources. Energy 268, 126617.

Hasanuzzaman, M., Zubir, U.S., Ilham, N.I., Seng Che, H., 2017. Global electricity demand, generation, grid system, and renewable energy polices: a review. WIREs Energy Environ. 6.

Anon Space Energy Initiative.

Ren, X.-N., Ge, C.-C., Chen, Z.-P., Irfan, 凡, Tu, Y., Zhang, Y.-C., Wang, L., Liu, Z.-L., Guan, Y.-Q., 2023. Energy conversion materials for the space solar power station *Chinese*. Phys. B 32, 078802.

Bidkar, R., 2012. Space Based Solar Power (SBSP): An emerging technology. *IEEE 5th India Int. Conf. Power Electron. (IICPE)* (IEEE) *2012*, 1–4.

Li, X., Duan, B., Song, L., Yang, Y., Zhang, Y., Wang, D., 2017a. A new concept of space solar power satellite. Acta Astronaut 136, 182–189.

Verduci, R., Romano, V., Brunetti, G., Yaghoobi Nia, N., Di Carlo, A., D'Angelo, G., Ciminelli, C., 2022. Solar Energy in Space Applications: Review and Technology Perspectives. Adv. Energy Mater. 12.

Gosavi, S.S., Mane, H.G., Pendhari, A.S., Magdum, A.P., Deshpande, S., Baraskar, A., Jadhav, M., Husainy, A., 2021. A Review on Space Based Solar Power. J. Therm. Energy Syst. 6, 16–24.

Wood, L.W., Gilbert, A.Q., 2022. Space-based Solar Power as a Catalyst for Space Development. Space Policy 59, 101451.

Jenkins, L.M., 2011. Concepts for demonstration of wireless power transfer for Space-Based Solar Power. In: *Aerospace Conference* (IEEE), *2011*, pp. 1–5.

Li, X., Duan, B., Song, L., Zhang, Y., Xu, W., 2017b. Study of Stepped Amplitude Distribution Taper for Microwave Power Transmission for SSPS. IEEE Trans. Antennas Propag. 65, 5396–5405.

Jaffe, P., McSpadden, J., 2013. Energy Conversion and Transmission Modules for Space Solar Power. Proc. IEEE 101, 1424–1437.

Powell, J., Paniagua, J., Maise, G., 2002. Potential use of high temperature superconductors in satellite power transmission and distribution systems. *AIP Conference Proceedings* (AIP), pp. 1168–1177.

Chiu, P.T., 2023. Space applications of III-V single- and multijunction solar cells. Photovoltaics for Space. Elsevier, pp. 79–127.

De Oliveira Lorenzi, J., Neves Micha, D., 2023. Optimization of Multi-Junction Solar Cells for the Orbit of Mars. J. Integr. Circuits Syst. 18, 1–6.

Liu, S., Qian, Y., Lin, Y., Sun, L., Zhu, Y., Li, D., 2024. Multilayer anti-reflective coating with ultra-low refractive index SiO2 nanopillars for high efficiency multi-junction GaAs solar cells. Sol. Energy Mater. Sol. Cells 266, 112679.

Liu, W., Liu, Y., Yang, Z., Xu, C., Li, X., Huang, S., Shi, J., Du, J., Han, A., Yang, Y., Xu, G., Yu, J., Ling, J., Peng, J., Yu, L., Ding, B., Gao, Y., Jiang, K., Li, Z., Yang, Y., Li, Z., Lan, S., Fu, H., Fan, B., Fu, Y., He, W., Li, F., Song, X., Zhou, Y., Shi, Q., Wang, G., Guo, L., Kang, J., Yang, X., Li, D., Wang, Z., Li, J., Thoroddsen, S., Cai, R., Wei, F., Xing, G., Xie, Y., Liu, X., Zhang, L., Meng, F., Di, Z., Liu, Z., 2023. Flexible solar cells based on foldable silicon wafers with blunted edges. Nature 617, 717–723.

Cai, W., Yang, T., Liu, C., Wang, Y., Wang, S., Du, Y., Wu, N., Huang, W., Wang, S., Wang, Z., Chen, X., Feng, J., Zhao, G., Ding, Z., Pan, X., Zou, P., Yao, J., Liu, S., (Frank), Zhao, K., 2023. Interfacial Engineering for Efficient Low-Temperature Flexible Perovskite Solar Cells. Angew. Chem. 135.

Qian, M., Zhang, Y., Mao, X., Gao, Y., Xuan, X., Wu, M., Niu, Y., Gong, S., 2023. Flexible photoelectronic material device and investigation method for space applications. Prog. Aerosp. Sci. 139, 100901.

Sato, K., Hayashi, K., Ohmatsu, K., Fujikami, J., Saga, N., Shibata, T., Isojima, S., Honjo, S., 1997. HTS large scale application using BSCCO conductor. IEEE Trans. Appl. Supercond. 7, 345–350.

Morandi, A., 2015b. HTS dc transmission and distribution: concepts, applications and benefits. Supercond. Sci. Technol. 28, 123001.

Sumption, M.D., Murphy, J., Susner, M., Haugan, T., 2020. Performance metrics of electrical conductors for aerospace cryogenic motors, generators, and transmission cables. Cryog. (Guildf.) 111.

Kottonau, D., Sousa, W.T.B., de, Bock, J., Noe, M., 2019. Design Comparisons of Concentric Three-Phase HTS Cables. IEEE Trans. Appl. Supercond. 29, 1–8.

Stamm, T., Cheetham, P., Kim, C.H., Pamidi, S.V., 2020. Superconducting Power Cable Design with Hybrid Cryogenic Media - Gaseous Helium for Cooling and Liquid Nitrogen for Dielectric Insulation. Electr. Insul. Conf. (EIC) *2020*, 22–26.

Bruzek, C.E., Allais, A., Dickson, D., Lallouet, N., Allweins, K., Marzahn, E., 2014. Superconducting DC cables to improve the efficiency of electricity transmission *Eco-friendly Innovations in Electricity Transmission and Distribution Networks*. Elsevier, pp. 135–168.

Nolan S., Jones C.E., Norman P.J. and Burt G.M. 2022 Sizing of Superconducting Cables for Turbo- Electric Distributed Propulsion Aircraft using a Particle Swarm Optimization Approach *IEEE Transactions on Transportation Electrification* **Early acce**.

Norris, W.T., 1970. Calculation of hysteresis losses in hard superconductors carrying ac: isolated conductors and edges of thin sheets. J. Phys. D. Appl. Phys. 3, 489.

Glowacki, J., Goddard-Winchester, M., Badcock, R., Long, N., 2020. Superconducting magnetic energy storage for a pulsed plasma thruster. AIAA Propuls. Energy Forum 24–28.

Ladner, D.R., 2011. Performance and Mass vs. Operating Temperature for Pulse Tube and Stirling Cryocoolers. Cryocoolers 16, 633–644.
Hahn, D.W., Özişik, M.N., 2012. Heat Conduction. Wiley.
de Sousa, W.T.B., Shabagin, E., Kottonau, D., Noe, M., 2021. An open-source 2D finite difference based transient electro-thermal simulation model for three-phase concentric superconducting power cables. Supercond. Sci. Technol. 34, 015014.
De Sousa, W.T.B., Shabagin, E., Kottonau, D., Noe, M., 2020. An open-source 2D finite difference based transient electro-thermal simulation model for three-phase concentric superconducting power cables. Supercond. Sci. Technol. 34.
Musso, A., Angeli, G., Bocchi, M., Luigi, P., Breschi, M., 2022a. A Method to Quantify Technical-Economic Aspects of HTS Electric Power Cables. IEEE Trans. Appl. Superconductivity2 32, 1–16.
Lee, C., Choi, J., Yang, H., Park, M., Iwakuma, M., 2019. Economic evaluation of 23 kV tri-axial HTS cable application to power system. IEEE Trans. Appl. Supercond. 29, 5–11.
Politano, D., Sjostrom, M., Schnyder, G., Rhyner, J., 2001. Technical and economical assessment of HTS cables. IEEE Trans. Appl. Supercond. 11, 2477–2480.
Li, Ren, Yuejin, Tang, Jing, Shi, Liang, Li, Jingdong, Li, Shijie, Cheng Cheng, 2009. Techno-economic feasibility study on HTS power cables. IEEE Trans. Appl. Supercond. 19, 1774–1777.
Lee, D., Jo, H.-C., Joo, S.-K., 2016. Economic evaluation method for fault current limiting superconducting cables considering network congestion in a power system. IEEE Trans. Appl. Supercond. 26, 1–4.
Yuan, W., Venuturumilli, S., Zhang, Z., Mavrocostanti, Y., Zhang, M., 2018. Economic Feasibility Study of Using High-Temperature Superconducting Cables in U.K.'s Electrical Distribution Networks. IEEE Trans. Appl. Supercond. 28, 1–5.
Morandi, A., Gholizad, B., Stieneker, M., Stagge, H., De Doncker, R.W., 2016. Technical and economical evaluation of dc high-temperature superconductor solutions for the grid connection of offshore wind parks. IEEE Trans. Appl. Supercond. 26, 1–10.
Yazdani-Asrami, M., Seyyedbarzegar, S.M., Zhang, M., Yuan, W., 2022a. Insulation materials and systems for superconducting powertrain devices in future cryo-electrified aircraft: Part I—material challenges and specifications, and device-level application. IEEE Electr. Insul. Mag. 38, 23–36.
Yazdani Asrami, M., Sadeghi, A., Atrey, M., 2022. Selecting a cryogenic cooling system for superconducting machines: general considerations for electric machine designers and engineers. Int. J. Refrig. 140, 70–81.
Radebaugh, R., 2004. Refrigeration for superconductors. Proc. IEEE 92, 1719–1734.
Anon Robinson HTS Wire Critical Current Data Base.
Yazdani-Asrami, M., Sadeghi, A., Atrey, M.D., 2022b. Selecting a cryogenic cooling system for superconducting machines: General considerations for electric machine designers and engineers. Int. J. Refrig. 140, 70–81.
Musso, A., Angeli, G., Bocchi, M., Ribani, P.L., Breschi, M., 2022b. A Method to Quantify Technical-Economic Aspects of HTS Electric Power Cables. IEEE Trans. Appl. Supercond. 32, 1–16.
Yazdani-Asrami, M., Sadeghi, A., Song, W., Madureira, A., Murta-Pina, J., Morandi, A., Parizh, M., 2022c. Artificial intelligence methods for applied superconductivity: material, design, manufacturing, testing, operation, and condition monitoring. Supercond. Sci. Technol. 35, 123001.
Yazdani-Asrami, M., 2023. Artificial intelligence, machine learning, deep learning, and big data techniques for the advancements of superconducting technology: a road to smarter and intelligent superconductivity. Supercond. Sci. Technol. 36, 084001.
Gonen, T., 2009. Electrical Power Transmission System Engineering. CRC Press.
Burkart, R.M., Kolar, J.W., 2017. Comparative Life Cycle Cost Analysis of Si and SiC PV Converter Systems Based on Advanced η- ρ-σ Multiobjective Optimization Techniques. IEEE Trans. Power Electron 32, 4344–4358.
Domingues-Olavarria, G., Fyhr, P., Reinap, A., Andersson, M., Alakula, M., 2017. From Chip to Converter: A Complete Cost Model for Power Electronics Converters. IEEE Trans. Power Electron 32, 8681–8692.
Burkart, R., Kolar, J.W., 2013. Component cost models for multi-objective optimizations of switched-mode power converters. In: IEEE Energy Conversion Congress and Exposition, *2013*. IEEE, pp. 2139–2146.
Ives, R.L., Read, M., Bui, T., Marsden, D., Collins, G., Freund, H., Ho, R., Higgins, L., Walker, C., Conant, J., Chase, B., Reid, J., Kroc, T., Yakovlev, V., Thangaraj, J.C.T., Dhuley, R.C., Potter, J., Jensen, A., Weatherford, B., Nanni, E.A., Tantawi, S., 2023. High efficiency, low cost, RF sources for accelerators and colliders. J. Instrum. 18, T05003.
Paz, H.P., Silva, V.S., Cambero, E.V.V., Araújo, H.X., Casella, I.R.S., Capovilla, C.E., 2019. A survey on low power RF rectifiers efficiency for low cost energy harvesting applications. AEU - Int. J. Electron. Commun. 112, 152963.